Space Science Center

Institute for the Study of Earth, Oceans, and Space (EOS)

10-22-1999

Coded-aperture x-ray/gamma-ray telescope for arc-minute localization of gamma-ray bursts

M L. Cherry
Louisiana State University - Baton Rouge

P P. Altice
Louisiana State University - Baton Rouge

D L. Band
University of California - San Diego

J Buckley
Washington University in St Louis

T G. Guzik
Louisiana State University - Baton Rouge

See next page for additional authors

Recommended Citation

Michael L. Cherry ; Peter P. Altice, Jr. ; David L. Band ; James H. Buckley ; T. Gregory Guzik ; Paul L. Hink ; S. C. Kappadath ; John R. Macri ; James L. Matteson ; Mark L. McConnell ; Terrence J. O'Neill ; James M. Ryan ; Kimberly R. Slavis ; John G. Stacy and Allen D. Zych "Coded-aperture x-ray/gamma-ray telescope for arc-minute localization of gamma-ray bursts", Proc. SPIE 3765, EUV, X-Ray, and Gamma-Ray Instrumentation for Astronomy X, 539 (October 22, 1999); doi:10.1117/12.366533; http://dx.doi.org/10.1117/12.366533

Authors

M L. Cherry, P P. Altice, D L. Band, J Buckley, T G. Guzik, P L. Hink, S C. Kappadath, John R. Macri, J L. Matteson, Mark L. McConnell, Terence J. O'Neill, James M. Ryan, K R. Slavis, J G. Stacy, and Allen Zych

A CODED-APERTURE X-RAY/GAMMA-RAY TELESCOPE FOR ARC-MINUTE LOCALIZATION OF GAMMA-RAY BURSTS

Michael L. Cherry[a], P. Parker Altice[a], David L. Band[b], James Buckley[c], T. Gregory Guzik[a], Paul L. Hink[c], S. Cheenu Kappadath[a], John R. Macri[d], James L. Matteson[b], Mark L. McConnell[d], Terrence J. O'Neill[e], James M. Ryan[d], Kimberly R. Slavis[c], J. Gregory Stacy[a,f], and Allen D. Zych[e]

[a] Louisiana State University, Baton Rouge, LA, 70803, USA
[b] University of California at San Diego, La Jolla, CA, 92093, USA
[c] Washington University, St. Louis, MO, 63130, USA
[d] University of New Hampshire, Durham, NH, 03824, USA
[e] University of California at Riverside, Riverside, CA, 92521, USA
[f] Southern University, Baton Rouge, LA, 70813, USA

ABSTRACT

MARGIE (Minute-of-Arc Resolution Gamma-Ray Imaging Experiment) will be a large-area ($\sim 10^4$ cm^2), wide field-of-view ($\sim 26°$ half-angle), hard X-ray/gamma-ray imaging telescope capable of providing accurate positions for faint gamma-ray bursts in near-real-time and of performing a sensitive survey of both steady and transient cosmic sources. The instrument is designed to image faint bursts at the low-intensity (high-redshift) end of the log N - log S distribution. MARGIE was recently selected by NASA for a mission-concept study for an Ultra Long Duration Balloon flight. We describe a program to develop an instrument based on the new detector technology of either cadmium zinc telluride room-temperature semiconductors or pixellated cesium iodide scintillators viewed by fast timing charge-coupled devices.

1. SCIENTIFIC OBJECTIVES

1.1 Rapid ArcMinute Localization of Gamma Ray Bursts

It has long been recognized that a key to unraveling the gamma ray burst mystery is the identification of burst counterparts at other wavelengths. Approximately ten optical transients have now been identified with gamma ray bursts, and nearly all of these identified with distant host galaxies. In the case of GRM 990123, the redshift of z = 1.6 identified with the optical transient[1,2] corresponds to an energy release (assuming isotropic emission) in excess of 2×10^{54} ergs, or 1.9 M_0c^2. Such a high energy release strains the models of the initial event, most of which are based on a catastrophic event at stellar death. The events with HST imaging all appear to be superimposed on galaxies, while neutron star merger models would suggest that (because of the kick provided by the supernova at the neutron star's birth) some of the bursts should occur well outside of the host galaxies. However, there is no evidence that bursts occur near the centers of the host galaxies, as might be expected if an AGN were the source of the gamma ray burst – and in the case of at least GRB 970228, the HST image[3] clearly shows the optical transient near the edge of the host galaxy. The source of the bursts is still very much a mystery, then, and the extremely large energy release is still a major challenge for the models.

A relativistic fireball with $\gamma = E/M > 100$ appears to be required in order to explain the lack of attenuation of the gamma rays due to pair production. The observed afterglows are reasonably consistent with the fireball model.

Nevertheless, the observation that the afterglows do not scale with the gamma ray intensities, and the lack of correlation between the ragged, irregular time structure of the gamma rays and the smooth power law decrease of the radio, optical, and X-ray afterglows suggest that the burst and the afterglow are separate events[4]. The gamma ray burst itself appears to be the result of internal shocks in the relativistically expanding ejecta; the prompt optical flash is due to the reverse shock travelling back through the dense ejecta; and the forward shock moving out through the interstellar medium produces the afterglow. Multiwavelength observations triggered by rapid localization and notification provide a wealth of information about the conditions in the shocked regions. The radio emission seems to show evidence for large event-to-event differences: The synchrotron peak frequency was significantly higher in GRB 971214 and GRB 970508 than in GRB 990123, suggesting that the two 1997 bursts were "high field" events compared to the "low field" 1999 event[5]-- although the radio signal may be connected to the prompt optical emission from the reverse shock, in which case the high-low field distinction is unnecessary. Beaming may show up as a steepening of the spectrum with time: If the emission is produced in a jet of angular width θ, then a decrease in the intensity is expected at the epoch where γ decreases below $1/\theta$. Kulkarni et al.[6] and Fruchter et al.[7] have suggested that they have seen such a decrease in the R-band flux (although not in the K-band!) for the January 23 event. On the assumption that they are seeing beamed emission, Kulkarni et al.[6] estimate a total energy release $\sim 10^{53}$ erg, significantly less than the 2×10^{54} ergs derived from the assumption of isotropic emission. Finally, Sari and Piran[4] point out that in the case of a thin shell of ejected material (corresponding to a short gamma ray burst), where the prompt optical emission can be separated from the gamma ray emission, the time at which the shell begins to decelerate is related to the initial Lorentz factor. In the case of GRB 990123, where the optical emission from the reverse shock was clearly distinguished from the γ-ray burst, Sari and Piran suggest $\gamma_o \sim 200$. The richness and complexity of the fireball phenomenon, and the apparent differences between events, require a large statistical sample of bursts in order fully to unravel what is going on in these spectacular events. MARGIE is intended to be a large area (10^4 cm^2), wide field of view (central detector with 8° half-width FOV, four side detectors with 26° half-width FOV), and good angular resolution (2'-4' geometric resolution) telescope designed to observe 30-40 gamma ray bursts in a 100 day balloon flight with sufficient signal-to-background to permit position determinations to within 1'. A population of 30 bursts with good position information, most of them near the faint end of the log N-log S distribution, with locations disseminated rapidly via the Galactic Coordinate Network (GCN) should lead to significantly more optical transients than the handful detected to date, and a corresponding larger sample of counterparts.

1.2 Hard X-ray Mapping of the Diffuse Emission from the Galactic Plane

The most recent report of NASA's Gamma Ray Working Group outlined a plan for the next years that included a hard X-ray (<200 keV) survey camera as a high priority item. The basis for promoting a hard X-ray survey instrument was largely that the most recent such survey was conducted with the HEAO-1 mission, more than 20 years ago. Since then most of the information we have collected about the hard X-ray sky has come from balloon instruments on day-long flights, from occultation monitoring of strong point sources using BATSE on CGRO, from investigations of point sources with the OSSE instrument on CGRO, and from partial sky surveys with moderate spatial resolution (~13') by the SIGMA instrument on GRANAT.

With MARGIE's wide field-of-view (central detector with 8° half-width FOV, four side detectors with 26° half-width FOV) and 2-4 minute of arc spatial resolution, MARGIE is an ideal instrument to perform hard X-ray mapping of the diffuse emission from the Galactic Plane. This is a difficult measurement that requires a wide FOV imaging instrument. For a coded aperture device, this implies a FOV considerably larger than the angular extent perpendicular to the Plane. We do not know how wide the Plane is at 100 keV. The ability of OSSE to image the Galactic 511 keV emission showing the "positron fountain" has produced new challenges to understanding positron production and transport in the Galaxy[8]. Similarly, imaging at lower energies (100-200 keV) could reveal new features of the Galaxy due to sources of electron bremsstrahlung and the positron continuum radiation. It took years of OSSE observations (with their small field of view) to construct the "fountain" image. MARGIE's wide-field data could easily complement those of INTEGRAL with its much smaller field of view and could even provide the INTEGRAL team with some directions for fruitful observations. Unfortunately, the distribution of annihilating positrons may not be a good indicator of the distribution of the energetic electrons (<1 MeV) which would be responsible for the hard X-ray diffuse Galactic emission. A wide FOV hard X-ray camera may therefore be useful in mapping the distribution of the ~100 keV electrons. This distribution would have important implications for the energy content of the galactic cosmic rays[9]. MARGIE also should be able to confirm the 511 backscatter line reported at 160 keV from the direction of the Galactic Center (e.g. Lingenfelter and Hua[10]) and, if it is real, determine its location with improved precision and accuracy. No other instrument has provided the combination of wide field of view and angular resolution to perform this

540

measurement properly. The development of an instrument with the capabilities of MARGIE will represent an important step forward in our understanding of the high-energy sky.

2. INSTRUMENT DESCRIPTION

We plan to construct a sensitive, large field-of-view, high angular resolution, hard X-ray/gamma ray telescope capable of observing gamma ray bursts and point sources with <1′ resolution on a 100-day Ultra Long Duration Balloon (ULDB) mission. MARGIE will be designed to take full advantage of the weight, power, and telemetry capabilities appropriate for a ULDB mission. The current instrument design consists of five coded aperture γ-ray telescopes: a central telescope with 1892 cm^2 of detector area, 1.9′ angular resolution, and 8.3° half-angle FOV; and four side-looking telescopes, each with 1945 cm^2 detector area, 3.8′ resolution, and 26.1° FOV. The five γ-ray telescopes will be surrounded by 10^5 cm^2 of 1 cm thick NaI active anticoincidence shields designed both to provide shielding from background and to provide additional sensitive detector area for faint γ-ray bursts. The total instrument mass is 990 kg. The total instrument power requirement is 760 W. An instrument schematic is presented in Figure 1.

MARGIE will fly at approximately the same time as INTEGRAL, and will provide far more burst sensitivity and angular resolution than either INTEGRAL or HETE. MARGIE will fly after the LIGO-1 gravity wave detector becomes operational, and will provide complementary γ-ray burst observations for LIGO, for the SuperKamiokande neutrino detector, and for optical transient searches. A fast trigger-telemetry-analysis-notification system will be implemented to notify ground-based and satellite observers about MARGIE burst detections and locations. MARGIE will be a follow-on to the extremely successful BeppoSAX mission but with significantly increased sensitivity and source-location capability.

The new technologies under development for use in MARGIE are described briefly in Section 2.1. The overall instrument concept for MARGIE is summarized in Section 2.2. The coded aperture mask is described in Section 2.3. In Section 2.4 we describe the central detectors: In Section 2.4.i we review the status of CZT development, and in Sections 2.4.ii and 2.4.iii we then describe the segmented CsI scintillator arrays and CCDs adopted as an alternative to CZT for the initial MARGIE design. We will be working in parallel on both the CZT (UCSD, UNH, UCR) and CsI-CCD (LSU, SU) technology during the mission study and expect to make a final decision between the two at the end of the concept study.

2.1 New Technology Development

The key enabling technology for MARGIE is the central detector. In order to obtain the fine-grained position resolution required in the plane of the central detector, two new position-sensitive γ-ray detector technologies are under development for use in MARGIE. The central detector will consist of five two-dimensional arrays of either 0.3 mm pitch cadmium zinc telluride (CZT) strip detectors or 0.5-0.9 mm pitch segmented cesium iodide (CsI) scintillator. The CsI scintillators will each be viewed by a Bi-Directional Charge Coupled Device (CCD) array designed for low-noise spectroscopy and fast timing (10 µs) applications.

Significant effort has been expended recently by our groups[11,12,13] and by others[14] on cadmium zinc telluride, a room-temperature semiconductor which, with some additional development, has the potential to provide a very suitable central detector for MARGIE. We have demonstrated better than 200 µm resolution with CZT strip detectors up to 1.5 mm thick[11], shown <8% (FWHM) energy resolution for 122 keV X-rays[11], presented designs for the required readout electronics[13], and measured a surprisingly low CZT background in two balloon flights[15]. There are problems with CZT, however, in particular the issue of fabrication of large-scale arrays. We are therefore pursuing an alternate development as well: pixellated CsI coupled to fast CCDs[16]. Custom application-specific-integrated-circuits (ASICs) will be provided for the CCD readout by Suni Imaging Microsystems (the CCD fabricator) and for the CZT by either Oak Ridge National Laboratory or Nova R&D. The central detectors are described in Section 2.4.

The coded aperture mask will consist of five uniformly redundant arrays photolithographically etched from tungsten. The masks will have 0.5-0.9 mm pixels and 0.5-5 mm thickness, corresponding to >10^7 individual cells. The etching procedures (including the details of acid concentrations, etch rates, material cleaning procedures, material selection,

etc.) have been developed on a series of prototype masks. The mask fabrication is described in Section 2.3.

2.2 MARGIE Instrument Concept

The essential components of the MARGIE coded aperture imager[17] are the mask, the CsI/CCD or CZT central detector, and the shields. As shown in Figure 1, MARGIE consists of five separate telescopes. The central telescope has an (87 cm)^2 x 5 mm thick tungsten mask viewed by an 1892 cm^2 CsI/CCD or CZT array with (0.8 mm)^2 pixels at a mask-detector separation of 150 cm. The central telescope is designed for high resolution (1.9′), narrow (8.3° half angle) FOV measurements of point sources in addition to gamma ray bursts. The four side telescopes (each with 88 x 88 cm^2 x 0.5 mm thick masks, a 1945 cm^2 detector array, 0.5 mm pixels, and 45 cm mask-detector separation) provide good sky coverage (26.1° half angle FOV, each with 3.8′ resolution) for gamma-ray bursts and additional sensitivity for point sources. Plastic charged particle scintillators covering the masks provide an anticoincidence veto for charged cosmic rays; and 1 cm thick NaI side shields attenuate atmospheric background photons, veto charged particles, and provide a large area for detecting gamma ray bursts at the low-intensity end of the log-N – log-S distribution.

The coded aperture (or "multi-pinhole") technique works by allowing an absorbing mask to cast a shadow pattern on a position-sensitive detection plane (e.g., Caroli et al.[18], Skinner e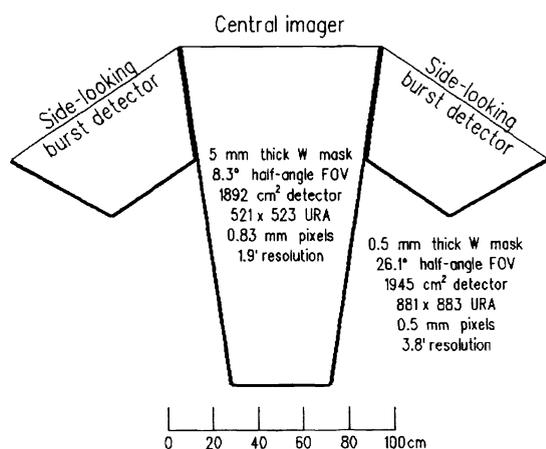t al.[19]). With a proper choice of mask pattern to minimize artifacts from the imaging process, the encoded pattern can then be processed to reproduce an image of the sky. The MARGIE mask design will be based on the uniformly redundant array (URA) patterns that have been successfully used in several previous experiments. The standard approach is to fabricate a mask using a 2 x 2 mosaic of the basic N x M URA pattern. In this configuration, the detection plane is the same size as the basic URA pattern. This design insures that no ambiguities are introduced into the imaging process. Several interrelated parameters must be considered in designing an imaging system. The angular resolution corresponds to the angular size of a mask element as seen from the detection plane, and so is dictated by the mask element size and the mask-detector separation. In order to achieve this level of angular resolution, however, the detector must be able to resolve the individual mask elements in the projected pattern; i.e., it must be able to locate events with an accuracy no larger than the mask element size. The exact ratio between detector spatial resolution and mask element size has an important effect on the signal-to-noise (S/N) ration in the reproduced image[20,21]. For a fixed element size, improved spatial resolution results in an improvement in the imaging S/N. One can think of this as

Figure 1. Schematic of MARGIE γ-ray telescope. Instrument will consist of a high resolution central imager and four wide-field-of-view side imagers. For clarity, only two of the side-looking elements are shown here.

an improvement in the ability of the detector to define the shadow produced by the mask. Any technology which improves the detector plane spatial resolution can therefore lead to an improvement in telescope sensitivity.

The mask element geometry is defined by the mask thickness and the mask element size (or width). The thickness must be sufficient to attenuate photons (hence, modulate the incident flux) in the desired energy range. On the other hand, the mask thickness must be limited so as to maintain uniformity of transmission for off-axis sources. (For thick masks, the resulting shadow may become distorted for sources at large off-axis angles.) In general, a greater FOV requires a smaller thickness-to-width ratio. Details of the MARGIE imaging system design are discussed in McConnell et al.[17].

2.3 Coded Aperture Mask

We have developed and tested the procedures for producing large coded aperture tungsten masks using relatively straightforward photolithographic etching techniques. An X-ray image of a prototype mask, taken with 40--50 keV X-rays from a dental X-ray machine using a segmented CsI microfiber array[22] and CCD camera, is shown in Figure 2. A reconstructed image of a light source observed in the laboratory using this mask is shown in Figure 3. Energetic

542

photons and cosmic ray particles striking the tungsten will produce fluorescence photons at an energy just below that of the tungsten K-edge. In order to attenuate the tungsten fluorescence photons, a graded mask will be used. We are still investigating various options for the grading material(s) and thicknesses. The choice will be dictated by the physical
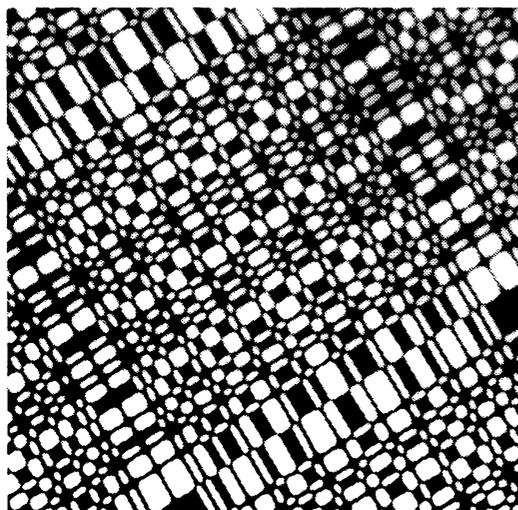

Figure 2. X-ray image of an etched tungsten mask obtained with a 1 mm thick CsI microfiber array and a CCD camera. The mask is a 71 x 73 URA pattern with 0.5 mm thickness and 0.5 mm minimum pixel dimensions[17].
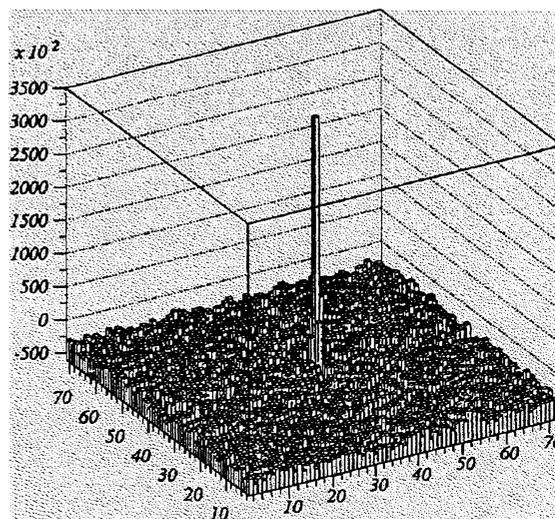

Figure 3. Reconstructed sky image based on test results with optical light beam illuminating 71 x 73 mask[17].

properties, ease of handling, cost of the material, and imaging performance. Tin and silver foils, for example, are both potentially useful in this regard. An alternative to the silver/tin foil is a thin painted layer of cerium oxide. Cerium has a K-edge at 40 keV and a low neutron cross section, and cerium oxide is cheap and readily available (although care must be taken to remove thorium impurities); we are currently investigating other rare earth compounds as well. Our initial sensitivity estimates incorporate a W-Ag mask. A thin layer of plastic scintillator will be placed below the mask for mechanical support and to provide a means of rejecting charged particles.

2.4 Central Detector

2.4.1 Cadmium Zinc Telluride CZT, or CdZnTe, is an alloy of CdTe and ZnTe, typically in the ratio 9:1, i.e., $Cd_{0.9}Zn_{0.1}Te$. It is a "room temperature" solid state detector material because its wide band gap, 1.6 eV, gives it high bulk resistivity at room temperature, $\sim 10^{11}$ ohm-cm, and correspondingly low leakage currents and shot noise. These properties, plus a mean atomic number ~ 50 and relatively high density, 5.8 g/cm^3, make it a desirable material for position-sensitive X-ray detectors. Below 250 keV the photoelectric effect dominates X-ray interactions, and the absorption coefficient at 100 keV is 0.9 mm^{-1}. Thus, compact, position-sensitive detectors are possible. Detectors up to 5-10 mm thick are available, although the large areas of MARGIE and production yield of thick detectors will probably require thicknesses of no more than ~ 3 mm, giving an efficiency of 55% at 200 keV. Since it is not necessary to use blocking-type electrical contacts, the same contact technique may be used for both the anode and cathode. Sputtered gold or platinum is often used. Contacts as fine as 100 μm are routinely fabricated.

Position sensitivity may be obtained in two ways -- pixel readout or crossed strip readout. With pixel readout the normal configuration is for X-rays to enter the detector's cathode surface. Electron-hole pairs are produced when the X-rays interact, and the electrons drift to the anode under the influence of the applied bias. Pixel spatial response is achieved by using an anode which is a set of separate pixel-sized contacts, each connected to its own preamplifier and electronic chain. While this approach is practical when the number of pixels is small, a prohibitive number of electronic chains would be required for MARGIE. The alternative readout method is "crossed strip". Here the top and bottom detector faces each have a parallel set of strip electrodes with a pitch that determines the spatial resolution. The

543

sets are at right angles, so one set gives the x-position and the other gives the y-position of an X-ray interaction. It is necessary to have an electronic chain for each strip, but the total amount of electronic channels is greatly reduced from the pixel readout case, by a factor of 64 in our case. Hole trapping effects limit the charge collection at the cathodes, and therefore the anode signals are normally used for energy analysis. It is necessary, however, that the cathode signal be large enough to identify under which cathode an interaction occurred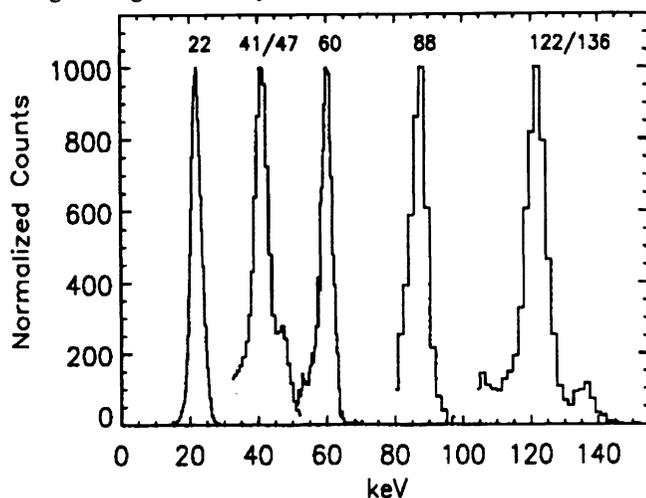. UCSD and UNH have been developing CZT detectors with crossed strip readout for hard X-ray detectors in astrophysics[11-13,23,24] and have demonstrated energy resolution of a few keV FWHM, an interaction depth-dependent cathode signal that is adequate to localize the event in all cases except for a few percent above 80 keV, and true pixel response with spatial resolution as fine as a few hundred microns for detectors of up to 2 mm thickness and up to 25 cm^2 area. Figure 4 gives an example of the spectral response obtained with discrete preamplifiers and laboratory electronics. The energy resolution at 60 keV is 4.2 keV, including electronic noise. Recently, good progress on the "RENA" ASIC readout chip has been reported[25]. UCSD has been working closely with the developer, NOVA R&D, on optimizing this 32-input device for CZT. An input-referred noise of 100 electrons rms is observed and an overall system resolution of 3 keV when coupled with a CZT detector.
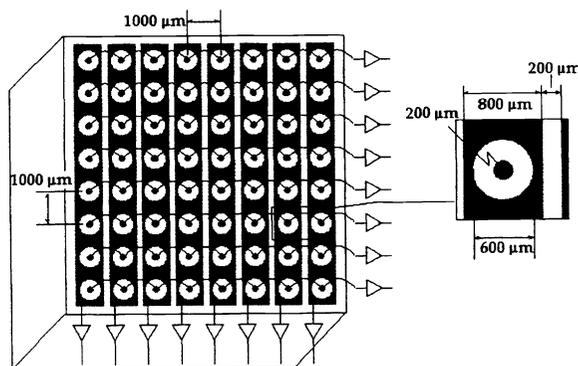

Figure 4. CZT spectra for five γ-ray line energies[13].

Figure 5. CZT imaging spectrometer with co-planar orthogonal anode strips[27].

Figure 5 illustrates a CZT strip detector approach developed at UNH and the University of Montreal employing a novel electrode configuration, orthogonal co-planar anodes patterned and interconnected to define an imaging area with 64 pixels (8⊗8) on a single CZT substrate[26,27]. The electrode geometry has non-collecting or controlling anode strips in one dimension and collecting anode pixels, interconnected in rows, in the orthogonal dimension. Electron motion near the anode plane results in induced charge signals on both collecting and non-collecting electrodes. The collecting anode pixels will be more positively biased than the non-collecting anode strips. The cathode, not shown, is a planar electrode on the opposite surface and is negatively biased with respect to both the collecting and non-collecting anodes. Each non-collecting strip and each orthogonal row of collecting pixels has a dedicated electronic channel for processing the induced charge signals. The energy is measured by the pulse height of the anode "pixels". The x-y coordinates of the γ-ray interaction are determined for each event by identifying the strip and the pixel row coincidentally detecting these signals. The orthogonal configuration retains the chief advantage that strip detectors have over pixellated configurations: achieving N^2 "pixels" with 2N electronic channels. Furthermore, computer simulations demonstrate improved energy resolution and detection efficiency advantages over conventional double-sided strip detectors over a broad energy range and that the z-dimension, or interaction depth, can be determined effectively from the shape of the non-collecting strip signal. An additional advantage over conventional strip detectors is that interconnections to the readout electronics are required on only one side, the anode side. We have identified technologies and processes that will permit highly reliable and low cost interconnections of the electrodes with the biasing and readout electronics. This will result in compact and rugged detector modules that can be arranged in arrays with little or no dead space between the modules.

544

Overall performance and background levels of CZT detectors at balloon altitudes were measured recently by UCSD and WU on two balloon flights at 105,000--109,000 feet. A 14 mm x 14 mm x 2 mm thick detector, with crossed strip readout, 500 μm pitch, and discrete preamplifiers, was tested. Energy resolution was identical to that in the laboratory, i.e., Figure 4. Background was measured for several shield configurations. In the October 15, 1997 flight 7 mm and 2 mm thick Pb/Sn/Cu graded passive shields were tested. On May 21-22, 1998 an ~5 cm thick CsI active shield was used at the sides and rear (140° aperture), and several shield and collimator schemes were placed in the aperture. One of these was similar to MARGIE, a 2 mm Pb/Sn/Cu passive shield with a 20° clear aperture. With a 10 MeV threshold, Figure 6 shows a background rate of ~5 x 10^{-4} cts/cm^2-s-keV in the 30-100 keV range[15]. The CsI shield was 5.5 cm thick, versus 1 cm NaI in the MARGIE concept, but this difference should have little effect below 100 keV since the transmission of MARGIE's NaI shield is <1% at these energies. At higher energies some X-rays will penetrate the NaI shield and there will be more background than shown in Figure 6.
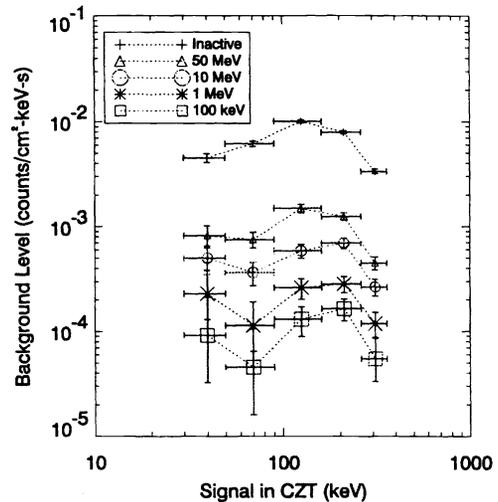

Figure 6. Background measured at balloon float altitude as a function of threshold in aCZT imaging spectrometer with co-planar orthogonal anode strips[15].

2.4.2 Segmented Scintillator Arrays CsI is an efficient X-ray/γ-ray scintillator. Nevertheless, 92% of 300 keV X-rays pass through 1 mm of CsI without interaction (96% at 500 keV). For a 1 cm thickness these fractions of unattenuated photons go down to 24% at 300 keV and 64% at 500 keV. In a uniform, homogeneous scintillator, however, as the detector thickness goes up, the spot size of the emitted scintillation light increases correspondingly: Since the light is emitted essentially isotropically, the spot size diameter is comparable to the detector thickness. One therefore has competing requirements: A thick detector is needed for high detection efficiency, while a thin detector is needed for good position resolution. The MARGIE position resolution requirements demand a spot size <0.5 mm.

CsI microfiber detectors offer a possible solution. Radiation Monitoring Devices, Inc. (RMD) has grown fiber arrays for us (see Figure 7) with thicknesses of 1 mm and 100 μm resolution[22,28], although it is difficult to grow fiber arrays with greater thicknesses. Such fiber arrays can be stacked (with somewhat reduced resolution), but a promising alternate approach is that of segmented metal matrices[29]. The idea is to start with a prefabricated metal mold similar to the composite honeycomb material used for a lightweight aircraft wing, and then inject molten CsI into the metal structure under vacuum. The temperature must be kept above 620° C (the CsI melting point) during the injection and then lowered in a controlled fashion after injection so as not to produce nonuniformities or voids. We will fabricate our metal matrices using techniques of deep X-ray lithography (LIGA) at LSU's Center for Advanced Microstructures and
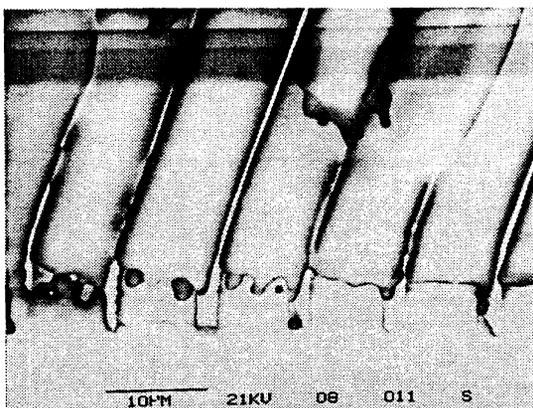

Figure 7. SEM closeup view of 300 μm film. The substrate pattern can be seen clearly at the bottom of the columns, with the well-separated CsI fibers growing up from the tops of the substrate pedestals[16].
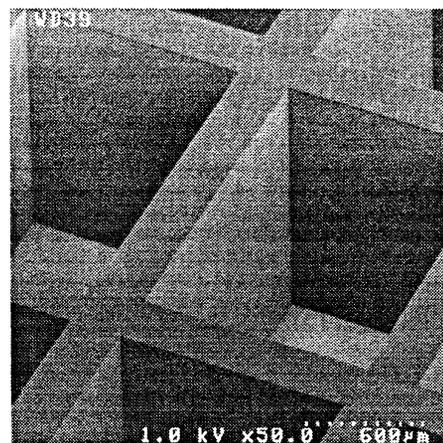

Figure 8. PMMA matrix produced at CAMD by LIGA[29].

545

Devices (CAMD). CAMD is a 1.4 GeV electron synchrotron and a leading U.S. center in deep X-ray lithography. The CAMD beamline will be used to produce very high aspect ratio (ratio of height to wall thickness ~100) matrices with pixel sizes ~500 μm and heights up to 1 mm, which can then be aligned and stacked together to produce a 1 cm high final structure. With a recently completed upgrade to the CAMD beamline, it may be possible to produce metal matrices with heights up to 1 cm without stacking. RMD will then perform the CsI vacuum injection.

The basic LIGA process begins with the creation of a mask. A chrome-on-quartz photomask from a 2-D CAD layout, similar to that for semiconductor manufacturing, is used to image the pattern on an X-ray transparent substrate (e.g. silicon or silicon nitride membrane or a beryllium substrate) through photolithography of a spin-coated photoresist layer. This step is followed by gold electroplating to form the absorber patterns opaque to X-rays. The resulting LIGA mask is used as for shadow printing with X-rays into a thick resist layer, typically an acrylic PMMA sheet bonded to a conductive substrate (e.g., a solid piece of metal or a silicon wafer with a plating base). During exposure, the X-rays produce chain scissions of the PMMA to reduce molecular weight in the exposed regions, which can selectively be dissolved in a developer (see Figure 9). After development of the resist, the cavities formed into the resist can be filled by electroplating. Candidate wall materials with a high atomic number include elemental metals such as gold, and alloys such as Ni-W. An alternative is to deposit tungsten into the PMMA mold by chemical vapor deposition. We will then inject the CsI melt into these 500 μm metallic matrices and stack layers together to form a composite of height 1 cm. Stacking with an alignment accuracy of approximately 5 μm can be achieved with standard mechanical alignment techniques. In order to achieve good light transmission through the stacked layers, the surfaces must be flat and optically coupled. The arrays will be polished, aligned, stacked, and tested for light yield and optical transmission.

2.4.3 Bi-Directional Fast Timing CCD The CsI scintillator output will be detected with a CCD. Standard CCDs are integrating devices operating at video rates (typically ~30 Hz). In a balloon-borne γ-ray telescope, however, the CCD must have time resolution better than the average time interval between cosmic ray hits on the veto shield (~10 kHz). In addition, if the CCD is to provide spectral information (e.g., on cyclotron lines, nuclear lines, the positron annihilation line, or spectral shapes), the time resolution must be good enough (and the noise must be low enough) to isolate single photons. We have therefore developed a Fast Timing Bi-Directional CCD with 10 μs timing resolution and 50 μm position resolution[30]. The Bi-Directional CCD employs a continuous, "bi-directional" readout scheme in which charge collected in alternate pixel columns is clocked separately to the top and bottom of the CCD chip (see Figure 9)[16]. By placing an amplifier at the top of each odd column and the bottom of each even column, eliminating the horizontal readout, and clocking continuously, we have demonstrated the expected performance in the laboratory (see, for example, Figure 10) on a set of Bi-Directional CCDs fabricated for us at the Orbit Semiconductors foundry, based on a design by Suni Imaging Microsystems, Inc. At 50 keV, the CsI produces 20 optical photons/keV which are detected with 35% quantum efficiency by the CCD. If each photon produces 1 electron and the signal is split over 4 pixels, then a 50 keV signal corresponds to approximately 90 e⁻/pixel. If the total (readout plus thermal) noise is 10 e⁻/pixel (rms), then the chance of spurious hits at the 9σ level simultaneously in 4 contiguous pixels in a 512 x 512 array is exceedingly small. An initial batch of Bi-Directional CCD prototypes has been produced by Suni at Orbit using a 1.2 μm, 2-metal, 2-poly process. The array utilizes two-phase
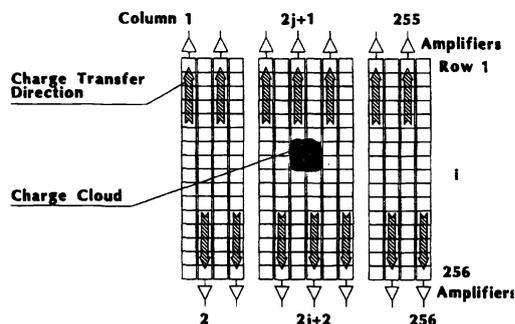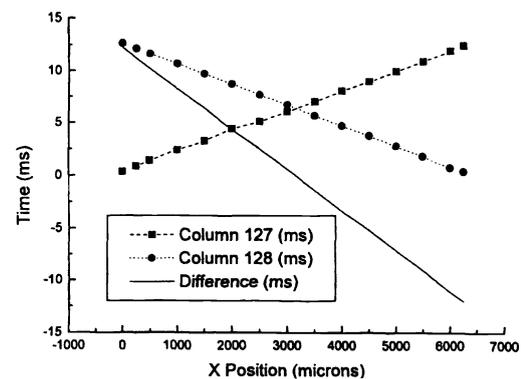

Figure 10. Plots of CCD voltage (converted to pulse height via an ADC) with optical light intensity are shown for both clocking directions. Both columns are linear with intensity, having approximately the same gain (but different voltage offsets).

Figure 9. Schematic view of the Bi-Directional CCD[16].

546

clocking, and is implemented as a collection of pixel columns with separate metal clock lines connecting to the polysilicon gates in each column. The direction of charge transfer is determined by the ordering of the polysilicon gates, which alternates from column to column. The independence of the clock lines guarantees that an electrical defect in a single column will not affect adjacent columns, and the closely-spaced metal lines between columns are driven identically, so metal-to-metal electrical shorts between these lines will have little effect. The primary on-chip amplifier is a source-follower type for simple low-noise operation.

For the initial prototypes, all the remaining readout electronics is external to the CCD. Proper readout chain design, however, is critical to low-noise CCD performance. For the Bi-Directional CCD, with an independent amplifier chain for each column, the readout circuitry will be implemented in 1.2 μm CMOS directly on the CCD. A preliminary design has been developed based closely on the designs for the SVX2 chip used at Fermilab[31,32] and the silicon detector on the ACE spacecraft cosmic-ray heavy-ion experiment. The next step will be to mate the readout and the CCD onto a single CMOS chip. Two readouts will service each CCD, with a total footprint $<(2.6 \text{ cm})^2$. Each readout ASIC will have 256 input channels (i.e., 256 for the top, 256 for the bottom of the CCD). Each readout channel will have an independent preamplifier, amplifier, double correlated sampling noise suppression, sample and hold, and ADC with a 30 μs event clocking rate. The ADC uses a low-power Wilkinson converter with a Gray code counter sensitive to both rising and falling edges of a common clock measuring time-above-threshold of a decreasing ramp of 256 channels. ADC resolution will be 9 bits, with power dissipation ~2 mW/channel for the full readout chain.

The readout chain will produce a string of digital ADC outputs at every clock cycle (nominally $t_{row} = 30$ μs). A fast digital signal processor will correlate each digital amplitude with appropriate identifier (column and CCD label) and time stamp (to label the row and, in order to determine the instantaneous pointing direction on a moving balloon platform, the event time). The signal processor will then write the ADC value/id tag/time stamp record in a continuous but sparsified data chain (of those outputs with ADC values above a preset threshold) to a fast, deep FIFO memory buffer. The FIFO output travels over the data bus to the on-board CPU, where a data frame is constructed and then written to disk or tape or sent to the telemetry module.

3. EXPECTED PERFORMANCE

3.1 Burst Sensitivity

Gamma ray burst sensitivity involves three principal experimental issues. First, we must detect a burst by measuring a statistically significant increase in the count rate. In a coded-mask detector, the fraction of the mask which is open directly affects the burst detection sensitivity: burst sensitivity increases as the square root of the open fraction. Second, MARGIE will localize the burst rapidly to disseminate the position as soon as possible. The initial burst localization will be calculated on board, although we will eventually send the data to the ground for more sophisticated analysis. Because the number of burst photons detected will be small relative to the number of open cells, the shadow pattern will be sparsely sampled, and back projection will be the most efficient deconvolution method. Third, we will want to study the burst spectrum and evolution. The scientific question in planning for a sky survey is the number of detectable sources expected. The practical issue is combining the counts taken with the detectors in different orientations since the gondola will not be stable enough to take long exposures of the same field, but instead the instantaneous orientation will have to be considered for every individual photon.

For an incoming photon flux ψ (photons/cm^2 s) at the top of the atmosphere, the observed count rate will be $\phi = <\alpha>/\psi$, where both ψ and ϕ are evaluated at the detection threshold in the fully coded region. Here $<\alpha>$ is the attenuation due to the atmosphere, the detector geometry, and the detector efficiency. The triggering sensitivity κ_b (in units of the number of standard deviations σ above background) for a detector with a detection area of A and a trigger time scale δt (the time over which the counts are accumulated) will be $\kappa_b = \phi A \, \delta t/(BA\delta t)^{1/2}$, where B is the background count rate in counts/cm^{2}s over the detector. Using the BATSE value of $\kappa_b = 5.5\sigma$, we expect a threshold flux of $\psi = \phi/<\alpha> = \kappa_b (B/A\delta t)^{1/2}/<\alpha>$. The attenuation is the product of the atmospheric attenuation α_{air}, the detector geometry α_d (a mask which is half open/half closed gives $\alpha_d = 0.5$), and the detector efficiency ε_d, all weighted by the energy dependence of the photon flux. The background consists of both internal B_{int} and aperture flux B_{ap} (i.e., the diffuse X-ray background observed through the mask). Based on the UCSD/Washington Univ. flight experience with CZT[15], we

547

approximate B_{int} as 10^{-4} counts/cm^2 s keV. B_{ap} consists of the diffuse background attenuated by both photoelectric absorption and Compton scattering, together with the atmospheric flux made up of the sum of scattered diffuse background photons and cosmic-ray induced emission. We use the Gruber parameterization of the diffuse background and take the atmospheric component from balloon measurements at 3 g/cm^2 overburden. The solid angle for the central imager is Ω_{cen} = 0.30 sr, and for the side detectors 1.60 sr, corresponding to (for the energy range 50 – 200 keV) B_{cen} = 6.21 x 10^{-2}/cm^2 s for the central telescope and B_{side} = 2.69 x 10^{-2}/cm^2 s for the side detectors. The resulting expected burst sensitivities are ψ_{cen} = 0.16 $\delta t^{-1/2}$ $\kappa_b/5\sigma$ cm^{-2} s^{-1} and ψ_{side} = 0.32 $\delta t^{-1/2}$ $\kappa_b/5\sigma$ cm^{-2} s^{-1} respectively.

BATSE detected essentially all bursts with peak fluxes greater than ψ_B = 0.3 cm^{-2}s^{-1} in the 50 – 300 keV energy band accumulated on the 1.024 s timescale. Using a MARGIE trigger threshold equal to ψ_B and the latest BATSE livetime for the 3B catalog (5.16 x 10^7 s, Meegan[38]), the expected number of bursts detectable by MARGIE will be N($>\psi_B$) = 472 yr^{-1} over the full sky. (This is less than the canonical 800 bursts per year which is often quoted. Since the early days of BATSE the instrument team realized that BATSE's livetime was greater than initially calculated. We note that while the 3B catalog has 1122 bursts, only 772 bursts met BATSE's trigger criteria on the 1.024 s timescale while a burst readout was not in progress; such a readout raises the burst threshold. The readout times are not included in the livetime. Thus there are two effects which diminish the burst rate: the greater livetime and the threshold of 0.3/cm^2 s.) The cumulative distribution is a -0.8 power law at the faint end, and therefore for the central detector $N_{cen}(>\psi_{cen})$ = N($>\psi_B$)(ψ_{cen}/ψ_B)$^{-.8}$ = 790 $\delta t^{-.4}$ ($\kappa_b/5\sigma$)$^{-.8}$ bursts/yr while for each of the four side detectors $N_{side}(>\psi_{side})$ = 444 $\delta t^{-.4}$ ($\kappa_b/5\sigma$)$^{-.8}$ bursts/yr, again over the full sky. The fully coded region for the central detector is (2 x 8.25°)^2 ~ 272 sq. degrees or a fraction f_{cen} ~ 7 x 10^{-3} of the entire sky, while for each of the side detectors the corresponding values are (2 x 26.1°)^2 ~ 2710 sq. degrees and f_{side} ~ 7 x 10^{-2}. During a mission of duration M = 100 d, the central telescope will detect N_{cen} = 1.4 $\delta t^{-.4}$ ($\kappa_b/5\sigma$)$^{-.8}$(M/100 d) bursts in the fully coded region while the individual side telescopes will detect N_{side} = 8.0 $\delta t^{-.4}$ ($\kappa_b/5\sigma$)$^{-.8}$(M/100 d) bursts. About 2/9 of the side detectors' fully coded regions overlap, and therefore the total number of bursts which should fall in some detector's fully coded region is ~25. The instrument can also detect and localize bursts in the partially coded regions. The partially coded regions of the central detector will overlap the areas viewed by the side detectors, while a fair fraction of the side detectors' partially covered regions will not overlap with other detectors. Therefore, MARGIE should detect and localize at least 40 bursts in a 100 day ULDB flight.

The ability to image the burst depends on the numbers of burst and background photons detected. The number of burst photons detected is N_{GRB} = $<\alpha>\psi AT_d\chi$ where T_d is the burst duration and χ is the ratio of the average and peak photon fluxes. Assuming the average burst has T_d = 10 s and χ = 0.3, then we expect N_{GRB} = 181 (380) γ rays in a threshold burst in the central (side) telescope and N_{tot} = N_{GRB} + BAT_d = 1360 (5580) total (background plus burst) photons, corresponding to a significance of 4.9 (5.1) σ for a threshold burst in the central (side) detector and 50 σ for the brightest burst expected. This significance can be translated into a probability of a fluctuation in a nonsource pixel which will equal or exceed the counts in the source pixel: The probability per pixel is less than 5 x 10^{-7} at threshold for both detectors, and less than 10^{-13} for the brightest expected burst for both detector types. However, the number of possible pixels on the sky is ~ 3 x 10^5 for the central detector and ~ 8 x 10^5 for each side telescope, and therefore there is a probability ~0.13 of a source-like fluctuation somewhere in the FOV at threshold, but an infinitesmal probability for the brightest bursts. Additional analysis on the ground will be required to reduce the number of spurious burst identifications near threshold; this is an unavoidable complication as the resolution improves and the number of pixels grows. The detection threshold for the planned MARGIE configuration is comparable to BATSE's for the side detectors, which cover a broad area, and about a factor of 2 deeper for the central detector, which covers a relatively small area. The MARGIE localization capabilities will be significantly better than BATSE.

3.2 Survey Capabilities

Since bursts are rare events, most of the mission will be used for a wide-field hard X-ray survey. We estimate the sensitivity by specifying the desired significance (e.g., κ_s = 5σ), and determining the strength of the source at the top of the atmosphere. The number of source photons will be N_s = $<\alpha>\psi AT_s$ where here T_s is the total integration time and ψ is the source flux at the top of the atmosphere integrated over the energy band of interest. Assuming the background dominates all resolvable sources, the total number of counts will be N_{tot} = BAT_s where again B is integrated over the energy band of interest. Note that N_{tot} should include contributions from all the sources in the FOV. The threshold

548

source flux is then $\psi = \kappa_s B^{1/2}/(\langle\alpha\rangle At_s)$. Numerically, ψ corresponds to $5.36 \times 10^{-4} \kappa_s/5\sigma\, (T_s/1\text{ day})^{-1/2}\,/cm^2$ s for the central detector, or $4.46\, \kappa_s/5\sigma\, (T_s/1\text{ day})^{-1/2}$ mCrab. At threshold, the number of source counts will be $1.6\,(3.4) \times 10^4$ $\kappa_s/5\sigma\, (T_s/1\text{ day})^{1/2}$ counts in the presence of $1.0\,(4.5) \times 10^7\,(T_s/1\text{ day})$ background events in the central (side) telescope.

The hard X-ray sky has not yet been well surveyed, and extrapolations from less sensitive, lower energy surveys are uncertain: Galactic sources usually have cutoffs steeper than $\psi \sim E^{-2}$, but type II AGN may be heavily absorbed at lower energies and thus will be more numerous at higher energies. Similarly, we can point at regions which are likely to have a higher hard X-ray density, such as the Galactic Center or the Magellanic Clouds. Nonetheless, we assume the detector has a source threshold of $\psi = \psi_m \kappa_{s,5} T_s^{-1/2}$, where $\kappa_{s,5} = \kappa_s/5\sigma$ and T_s is the observation time in units of a day, and take the all-sky cumulative source distribution to be $N(>\psi) = N_0(\psi/\psi_0)^{-\gamma}$ where $\gamma=1$ for Galactic sources and $\gamma=1.5$ for extragalactic sources. If the mission duration of M days is broken into N_{FOV} pointings of T_s days each, then the expected number of detected sources is $N_{det} = N_0 M/T_s^{1-\gamma/2} (\Delta\Omega_{FOV}/\Delta\Omega_{Sky}) (\psi_0/\psi_m)^\gamma$ where $\Delta\Omega_{FOV}$ is the solid angle of the detector and $\Delta\Omega_{Sky}$ is the solid angle of the entire sky. Clearly, with enough pointings, the whole sky will be covered, so for a mission of duration $M/T_s(\Delta\Omega_{FOV}/\Delta\Omega_{Sky})$ cannot be greater than 1. For the central detector this limits $T_s > 0.66$ d and for each side detector $T_s > 6.6$ d (neglecting unequal exposures, partially coded regions, etc.). The *HEAO-1/A4* catalog[37] had 65 Galactic and 8 extragalactic sources in an all-sky survey to a flux limit of 13 mCrab above 13 keV. The HELLAS (*Beppo-SAX*) 5-10 keV survey[38] gives a similar result for extragalactic sources. Assuming these results can be extrapolated to higher energies with a Crab spectrum, we expect $N_{det} = 232\,(M/100\text{ d})\,(T_s/10\text{ d})^{-1/2}$ and 65 $(M/100\text{ d})\,(T_s/10\text{ d})^{-1/4}$ Galactic and extragalactic sources respectively in the combined telescope.

Table 1. Characteristics of the MARGIE payload

Forward	Side	Total	
1	4	5	Number of telescopes
150	45		Mask to detector separation (cm)
521	881		URA dimension
87.0	88.2		Mask size (cm)
5	0.5		Mask thickness (mm)
36	4	51	Mask mass (kg)
1892	1945	9671	Detector area (cm^2)
1	1		Detector thickness (cm)
11	11	55	Detector mass (kg)
1	1		Shield thickness (cm)
3.57	3.57		Shield density (g/cm^3)
148	54	365	Shield mass (kg)
0.83	0.50		Pixel size (mm)
1.9	3.8		Resolution (minutes)
8.3	26.1		Half-angle field of view (degrees)
96	98	489	Telescope power (W)
		760	Total instrument power (W)
195	69	471	Telescope mass (kg)
		986	Total instrument mass (kg)

3.3 Instrument Characteristics

The characteristics of the instrument are summarized in Table 1. In comparison, we summarize here the characteristics of similar instruments, existing and planned. On BeppoSAX, the two Wide Field Cameras each have 5' angular resolution and 40° x 40° FOV, with a total area of 530 cm^2; the high energy PDS (Phoswich Detection System) covers the energy range 15-300 keV with 795 cm^2 of NaI and CsI scintillator[33]. INTEGRAL's spectrometer will have 330 cm^2 of germanium with 1.4° resolution and 5.6° FOV, and the imager will have 2500 cm^2 of CsI with 17' resolution and 3.2°

549

FOV[34]. HETE was designed to fly 120 cm^2 of NaI covering the energy range 6 keV to >1 MeV with a FOV of ~2π sr[35]. SWIFT will fly with a Burst Alert Telescope that has 5200 cm^2 of CdZnTe and will have ~2π sr FOV and a 22′ spatial resolution with an energy range of 10-150 keV and an X-Ray Telescope consisting of a CCD with 23′ FOV and 15″ spatial resolution at energies of 0.2-10 keV. BATSE, the largest burst detector currently flying, has 2.6 x 10^4 cm^2 of NaI and has a full sky FOV, but only 3° angular resolution[36]. By contrast, MARGIE will have 9.7 x 10^3 cm^2 of CsI, 10^5 cm^2 of active NaI shield, and 1.9′-3.8′ resolution.

In sum, the MARGIE instrument will be a large-area, wide field-of-view, hard X-ray/γ-ray imaging telescope capable of providing accurate positions for, and of characterizing the temporal and spectral behavior of, faint transient sources in near-real-time, for rapid counterpart searches. It will carry out sensitive surveys for both steady and transient cosmic sources over the course of a 100-day Ultra Long Duration Balloon flight, and detect, image, and localize to arcminute precision, faint bursts at the low-intensity (high-redshift) end of the γ-ray burst distribution.

ACKNOWLEDGEMENTS

REFERENCES

[1] J. Hjorth et al., GCN Notice 219 (1999).
[2] D. Kelson et al., IAU Circ. 7096 (1999).
[3] K.C. Sahu et al., Nature 387, 476 (1997).
[4] R. Sari and T. Piran, astro-ph/9901338 and astro-ph/9902009 (1999).
[5] T. Galama et al., astro-ph/9903021 (1999).
[6] S.R. Kulkarni et al., astro-ph/9902272 (1999).
[7] A. Fruchter et al., astro-ph/9902236 (1999).
[8] W.R. Purcell et al., Ap. J. 491, 725 (1997).
[9] J. Skibo and R. Ramaty, in Compton Gamma Ray Observatory (AIP Conf. Proc. 280), p. 70 (1993).
[10] R.E. Lingenfelter and X.M. Hua, Ap. J. 381, 426 (1991).
[11] J.R. Macri et al., Proc. SPIE 2859, 29 (1996).
[12] J.L. Matteson et al., Proc. SPIE 3115, 160 (1997).
[13] J.L. Matteson et al., Proc. SPIE 3446, 192 (1998).
[14] C.M. Stahle et al., Proc. SPIE 2859, 74 (1998).
[15] K.R. Slavis et al., Proc. 26th Intl. Cosmic Ray Conf., to be published (1999) and Proc. SPIE 3765, to be published (1999).
[16] M.L. Cherry et al., Proc. SPIE 2806, 551 (1996).
[17] M. McConnell et al., Proc. SPIE 2806, 349 (1996).
[18] E. Caroli et al., Space Sci. Rev. 45, 349 (1987).
[19] G.K. Skinner et al., Astrophys. Space Sci. 136, 337 (1987).
[20] P.M. Charalambous et al., Nucl. Instr. and Meth. in Phys. Res. A221, 56 (1984).
[21] I.D. Jupp et al., Nucl. Instrum. Meth. A345, 576 (1994).
[22] M.L. Cherry et al., Proc. 24th Intl. Cosmic Ray Conference, Rome 2, 45 (1995).
[23] O. Tousignant et al., Proc. SPIE 3115, 214 (1997).
[24] J.L. Matteson et al., Proc. SPIE 2859, 58 (1996).
[25] S.D. Kravis et al., Proc. SPIE 3445, 374 (1998).
[26] L.A. Hamel et al., Proc. Material Research Soc. Fall Meeting, Boston (1997) and Proc. SPIE 3768, to be published (1999).
[27] M. Mayer et al., Symp. On Radiation Measurements and Applications, Ann Arbor, to be published in NIM-A (1998).
[28] J. Gordon et al., X-ray and Ultraviolet Sensors and Appl., Proc. SPIE 2519, 2 (1995).
[29] S.A. Vasile et al., Proc. SPIE 2859, 94 (1996).
[30] M.L. Cherry and S.B. Ellison, U.S. Patent No. 5693968 (1997).
[31] S.A. Kleinfelder et al., IEEE Trans. Nucl. Sci. 35, 171 (1988).
[32] T. Zimmerman, IEEE Trans. Nucl. Sci. 42, 803 (1995).
[33] E. Costa et al., Nature 387, 783 (1997).
[34] C. Winkler, Astron. Astrophys. Suppl. Ser. 120C, 637 (1996).
[35] G. R. Ricker, in "All-Sky X-Ray Observations in the Next Decade," RIKEN, Japan, eds. M. Matsuoka and H. Kawai, 366 (1997).
[36] G.J. Fishman and C.A. Meegan, Ann. Rev. Astron. Astrophys. 33, 415 (1995).
[37] A. Levine et al., Ap. J. Suppl. 54, 581 (1984).
[38] F. Fiore et al., First XMM Workshop, to be published (1999).